

Study of open cluster King 13 using CCD VI, 2MASS and Gaia DR2 Astrometry.

Alok Durgapal¹, D Bisht², Geeta Rangwal¹, Harmeen Kaur¹, R. K. S. Yadav³

¹*Department of Physics, DSB Campus, Kumaun University, Nainital-263002, Uttarakhand, India*

²*Key Laboratory for Researches in Galaxies and Cosmology, University of Science and Technology of China, Chinese Academy of Sciences, Hefei, Anhui 230026, China*

³*Aryabhata Research Institute of Observational Sciences, Manora Peak Nainital 263 002, India*

Abstract

In this paper, we present astrophysical parameters of the open cluster King 13 based on the VI CCD and 2MASS JHK_s photometric data. This is a poorly studied cluster, for which new results have been found in the present work. To identify probable members, we use proper motion data from Gaia DR2 catalogue. The mean proper motion of the cluster is determined as -2.8 ± 0.2 and -0.88 ± 0.14 mas yr⁻¹ and cluster extent is derived as 3'.2. Using color-magnitude diagrams, we estimate the age and distance of the cluster as 510 ± 60 Myr and 3.84 ± 0.15 kpc respectively. Interstellar reddening $E(B - V)$ in the direction of the cluster is determined as 0.80 ± 0.2 mag using color-color diagram. Mass function slope of the cluster is found to be comparable with the Salpeter value. The total mass of this cluster is derived as $270 M_{\odot}$. The present analysis shows that King 13 is a dynamically relaxed cluster.

Keywords:

Star cluster - individual: King 13 - star: Astrometry, mass function, dynamical state, Galaxy: structure.

¹E-mail: alokdurgapal@gmail.com (Alok Durgapal); devendrabisht297@gmail.com (D. Bisht); geetarangwal91@gmail.com (Geeta Rangwal); harmeenkaur.kaur229@gmail.com (Harmeen Kaur); rkant@aries.res.in (R. K. S Yadav)

²Corresponding author; Tel:+86-15695691278

1. Introduction

Open clusters (OCs) are very helpful objects to understand the structure and stellar evolution of the Milky Way. Indeed, each cluster includes stars of different mass, which were formed in the same cloud, i.e. they share the same age and chemical composition. The structure of most OCs can be roughly described by two subsystems, the dense core and the sparse halo (Bonatto and Bica, 2009). OCs have become fundamental probes of Galactic disk properties by their location on Galactic disk (Lynga, 1982; Janes and Phelps, 1994; Friel, 1995; Piskunov et al., 2006; Carraro et al., 2010). The fundamental parameters of an open cluster e.g. distance, age and interstellar extinction can be estimated by comparing color-magnitude diagram (CMD) and color-color (CC) diagrams with the modern theoretical models. It is important to study the unexplored OCs to determine their properties with the aim of improving the picture of the Galactic disk.

King 13 is positioned at $\alpha = 00^h 10^m 06^s$ and $\delta = 61^\circ 10'$ (J2000.0), corresponding to Galactic coordinates $l = 117^\circ.96$ and $b = -1^\circ.3$. This object is located in the Perseus arm, in the second Galactic quadrant of Milky Way. Marx and Lehmann (1979) obtained UBV photographic photometry for King 13 and calculated its distance as 1.73 kpc. Subramaniam and Bhatt (2007) determined its distance as 3.10 ± 0.33 kpc and its age as 300 Myr, while Bukowiecki et al. (2011) estimated cluster distance as 2.96 ± 0.19 kpc and age as 794 Myr. Therefore, there is a difference in parameters from one study to another. So there is a need to re-visit this cluster and determine its parameters in a more accurate way, making use of new tools and data.

A new era in dynamical astronomy has begun with the second data release of the Gaia mission in 2018 April (Gaia Collaboration et al., 2016). In the present analysis, we used CCD photometric data in *VI* filters, 2MASS data in *JHK_s* filters and Gaia DR2 proper motion data to determine the fundamental and structural parameters of the cluster King 13.

The paper is organized as follows: Data reduction is presented in Section 2. Selection of cluster members is described in Section 3. Fundamental astrophysical parameters are estimated in Section 4. Study of luminosity, mass function and mass-segregation are given in Section 5. Finally, we concluded our study in Section 6.

2. Observational data and data reduction

The CCD broadband *VI* images for King 13, were collected using a 2K×2K CCD system at the f/13 Cassegrain focus of the 104 cm Sampurnanand telescope

located at ARIES, Manora peak, Nainital, India. The CCD used for the present observations has $24 \mu\text{m}$ square pixel size, resulting in a scale of $0''.36 \text{ pixel}^{-1}$ and a square field of view of $12'.6$ size. The CCD gain was $10 \text{ e}^-/\text{ADU}$ while the readout noise was 5.3 e^- . Log of observations is listed in Table 1. Observations were taken in 2×2 pixels binning mode to improve S/N ratio. The identification map of the observed region for King 13 is shown in Fig. 1. In this figure, the core and cluster regions are indicated by the inner and outer circle respectively.

Bias and twilight flats were also taken along with the target field. We have used IRAF software for the pre-processing of our observed CCD images. In this step, we have done bias subtraction, flat field correction and removal of cosmic rays from science images. The subsequent data reduction and analysis were done using the DAOPHOT software (Stetson, 1987). The stellar photometric routine of DAOPHOT was used for the instrumental magnitude determination. Both PSF and aperture photometry was carried out to find the instrumental magnitudes of the stars. The details of the processing of the images can be found in our previous papers (Pandey et al., 1997; Durgapal et al., 1997; Durgapal and Pandey, 2001; Bisht et al., 2016, 2019).

2.1. Photometric calibration

We observed the standard field SA 95 (Landolt, 1992) in V and I filters for calibrating the observational data of King 13. The 7 standard stars (SA95-41, 42, 43, 97, 102, 112, 115) used in the calibrations having brightness and color range $12.77 \leq V \leq 16.11$ and $-0.329 < (V - I) < 1.448$ respectively, thus covering the bulk of the cluster stars. For the extinction coefficients, we considered the values for the ARIES site (Kumar et al., 2000). The derived calibration equations using least square linear regression for converting the instrumental magnitude into the standard magnitude, are as follows:

$$v = V + Z_V + C_V(B - V) + k_V X \quad (1)$$

$$i = I + Z_I + C_I(V - I) + k_I X \quad (2)$$

where v and i are the instrumental and V and I are the standard magnitudes, X is the airmass. The color coefficients (C) and zero points (Z) for different filters are listed in Table 2. The errors in zero points using standard stars from Landolt SA 95 field and color coefficients are 0.01 mag.

The internal errors derived from DAOPHOT are plotted against V magnitude in Fig. 2. Photometric global (DAOPHOT+Calibrations) errors are also estimated,

which are listed in Table 3. For V filter, the error is 0.05 mag at $V \sim 17$ mag and 0.07 mag at $V \sim 20$ mag.

In Fig. 3, we present a comparison of present photometry with the photometric data of Glushkova et al. (2010). In this figure, the difference between the two photometries is plotted as a function of the present photometry. The dotted lines represent the zero difference between present photometry and photometry by Glushkova et al. (2010). This shows that most of the data points lie near the zero difference line so our photometric data is in good agreement with that of Glushkova et al. (2010). The mean difference and standard deviation per magnitude bin are also given in Table 4.

2.2. Gaia DR2 data

We used Gaia DR2 data (Gaia Collaboration et al., 2016) to select the cluster members and determine the mean proper motion of cluster King 13. This data consist of five parametric astrometric solution, which includes positions on the sky (α, δ), parallaxes and proper motion (PM) ($\mu_\alpha \cos \delta, \mu_\delta$) with a limiting magnitude of $G \sim 21$ mag. Parallax uncertainties are in the range of up to 0.04 milliarcsecond (mas) for sources at $G \leq 15$ mag and ~ 0.1 mas for sources at $G \sim 17$ mag. The uncertainties in the respective proper motion components are up to 0.06 mas yr^{-1} (for $G \leq 15$ mag), 0.2 mas yr^{-1} (for $G \sim 17$ mag) and 1.2 mas yr^{-1} (for $G \sim 20$ mag). The proper motion and their corresponding errors plotted against G magnitude are shown in Fig 2. This figure shows that errors in proper motion components are ~ 1.2 at $G \sim 20$ mag.

3. Mean proper motion and cluster membership

The contamination due to field stars always affects the determination of fundamental parameters of the cluster. Proper motion is one of the tools to remove those field stars from the cluster main sequence. We used Gaia DR2 proper motion and parallax data to separate cluster members from non member stars.

To see the distribution of member and non member stars, we plotted vector point diagram (VPD) in PMs $\mu_\alpha \cos \delta$ and μ_δ as shown in Fig 4. Corresponding V versus $(V - I)$ CMDs are also shown in top panels. The left panel shows all the observed stars, while the middle and right panel shows probable cluster members and field stars respectively.

We determined the average value of parallax for stars inside the circle of vector point diagram, by building a histogram of 0.15 mas bin as shown in Fig 6. The average value of parallax is determined as 0.26 ± 0.006 mas after incorporating

the zero point offset (-0.05 mas) as suggested by Riess et al. (2018). The cluster distance corresponding to the average parallax is obtained as 3.84 ± 0.15 kpc. This value is in good agreement with the distance estimated by Cantat-Gaudin et al. (2018).

We also used parallax of cluster stars along with the proper motion data to find true cluster members. A star is considered as probable member if it lies inside the circle of 0.7 mas yr^{-1} in VPD and has a parallax within 3σ from the mean cluster parallax. In this way we obtained a total 172 stars as probable cluster members for King 13. We have matched our members with Cantat-Gaudin et al. (2018) catalog as well. We have shown these matched stars with red open circles in the observed colour magnitude and color-color diagrams. In our previous analysis (Rangwal et al. (2019)), we clearly explained this method in detail. The CMD of the probable cluster members having PM error $\leq 1 \text{ mas yr}^{-1}$ are shown in the upper-middle panels of Fig 4. The main sequence of King 13 is clearly separated from the field stars.

To calculate the mean proper motion of King 13, we constructed histograms of proper motions and fitted their peaks with Gaussian functions (see Fig 5). We found -2.8 ± 0.2 and $-0.9 \pm 0.1 \text{ mas yr}^{-1}$ as mean proper motions in RA and DEC directions respectively. These proper motion values are very close to the values given by Cantat-Gaudin et al. (2018). By visual inspection, we define a circle of 0.7 mas yr^{-1} radius, around the cluster center in the VPD which defines our member selection criteria. The chosen radius is a boundary between losing cluster members with poor PMs and the inclusion of field stars.

4. Cluster structure and its fundamental parameters

4.1. Cluster structure

In order to investigate the cluster structure, the primary step is to find very precise center coordinates. For this, we have plotted the histogram of star counts in Right Ascension (RA) and Declination (DEC) using Gaia database. Our main aim is to estimate the maximum central density of the cluster. The cluster center is estimated by fitting Gaussian function of star counts in RA and DEC as shown in Fig 7, finding coordinates as $\alpha = 2.54 \pm 0.01$ deg and $\delta = 61.19 \pm 0.01$ deg. The cluster center in celestial coordinates is at $\alpha_{2000}=00^h 10^m 9.6^s$, $\delta_{2000}=61^\circ 11' 24''$. These coordinates are very close to the values given by Glushkova et al. (2010) and are also in good agreement with the center coordinates reported by Cantat-Gaudin et al. (2018).

To estimate the cluster extent, we established the radial density profile (RDP) of King 13. To construct RDP the observed area of the cluster is divided into many concentric circles. The number density, R_i , in the i^{th} zone is calculated by using the formula $R_i = \frac{N_i}{A_i}$, where N_i is the number of stars and A_i is the area of the i^{th} zone. RDP of the cluster King 13 is shown in Fig. 8. A smooth continuous line represents the fitted King (1962) profile, which can be expressed as:

$$f(r) = f_b + \frac{f_0}{1+(r/r_c)^2} \quad (3)$$

where f_0 is the central density, r_c is the core radius and f_b is the background density. The background density level with errors is shown with dotted lines in this figure. This RDP flattens at $r \sim 3.2$ arcmin and begins to merge with the background stellar density which can be seen in Fig. 8. Therefore, we consider 3.2 arcmin as the extent of this cluster. By fitting the King model to the cluster density profile, we estimated the values of central density, background density and core radius as $36.3 \pm 4.2 \text{ stars/arcmin}^2$, $16.04 \pm 0.3 \text{ stars/arcmin}^2$ and 0.6 ± 0.1 arcmin. These parameters are also listed in Table 5.

The density contrast parameter $\delta_c = 1 + \frac{f_0}{f_b}$ for the cluster is estimated as 2.8, which is smaller than the values ($7 \leq \delta_c \leq 23$) given for compact star clusters by Bonatto and Bica (2009). This shows that King 13 is a sparse cluster.

The tidal radius generally depends on the effects of Galactic tidal fields and subsequent internal relaxation dynamical evolution of clusters (Allen and Martos, 1988). To evaluate the clusters tidal radius, we have adopted the following relation as given by Jeffries et al. (2001)

$$R_t = 1.46 \times (M_c)^{1/3} \quad (4)$$

where R_t and M_c are the tidal radius and the total mass (see Sec. 5) of the cluster respectively. The estimated value of the tidal radius is found as 8.5 pc.

4.2. Interstellar extinction

The interstellar extinction and the ratio of total-to-selective extinction towards the cluster are very important for a proper use of photometric data. The value of interstellar extinction $E(B-V)$ in the direction of King 13 has been estimated using near-IR *JHK* data from 2MASS catalogue in combination with the optical data. We followed Persson et al. (1998) to convert K_s magnitude into K magnitude. We plotted $(J-K)$ versus $(V-K)$, $(J-K)$ versus $(J-H)$ and $(V-I)$ versus $(V-K)$ color-color diagrams which are shown in Fig. 9. The ZAMS by Bressan et al.

(2012) is fitted over the color-color diagrams as shown by the solid black line. We have also shown the shifted ZAMS also by dotted line in this figure. We have estimated $E(G_{BP} - G_{RP}) = 0.71 \pm 0.26$ and $A_G = 1.44$ for King 13 using optical data from Gaia database in G , G_{BP} and G_{RP} filters. The error in the calculated value of $E(G_{BP} - G_{RP})$ is the fitting error of ZAMS. With the help of this, errors in colour-excess are calculated in further transformations. We used the absorption ratio in the optical and infrared wavelengths to visual absorption from Cardelli et al. (1989). Using the transformation equations by Hensy (2018), we found the value of interstellar reddening $E(B - V)$ as 0.80 ± 0.2 . The shifted ZAMS provides $E(V - K) = 2.5$ mag, $E(J - K) = 0.48 \pm 0.6$ mag and $E(J - H) = 0.26 \pm 0.3$. We used the relations, $A_k = 0.618 \times E(J - K)$ (Mathis, 1990); $A_k = 0.122 \times A_v$ (Cardelli et al., 1989) and $A_v = R \times E(B - V)$ to estimate the value of A_v and R . Using the above relations we found the value of A_v as 2.43 and R as ~ 3.04 . Color excess ratios are calculated as $\frac{E(J-K)}{E(V-K)} \sim 0.19$ and $\frac{E(J-K)}{E(J-H)} \sim 1.84$, which are in good agreement with the normal interstellar extinction value as suggested by Cardelli et al. (1989).

4.3. Age and distance of the cluster

The metallicity, age and distance of King 13 have been estimated by comparing the observed CMDs with theoretical stellar evolutionary isochrones. For this purpose we adopted the isochrones of Bressan et al. (2012). The main-sequence of the cluster is well reproduced by isochrones with a nearly solar metallicity, $Z=0.012$, which have been adopted for the following analysis.

We surveyed different age isochrones to get the best fit with morphological features in V , $(V - I)$; V , $(V - K)$ and K , $(J - K)$ CMDs. To get a clear sequence in the CMDs, we consider only probable cluster members based on the cluster's VPD. In Fig. 10, we superimpose isochrones of different age ($\log(\text{age})=8.65$, 8.70 and 8.75) having $Z = 0.012$ in V , $(V - I)$; V , $(V - K)$ and K , $(J - K)$ CMDs. Assuming the brightest star as an evolved star, we found an age of 510 ± 60 Myr. The distance modulus for the cluster is found to be $(m - M) = 14.8 \pm 0.2$ mag which corresponds to a heliocentric distance of 3.75 ± 0.4 kpc. Present estimated distance of King 13 is 2.1 kpc higher than the previously derived value by Haroon et al. (2014) using 2MASS $JHKs$ data. The Galactocentric coordinates for the cluster are determined as $X = 3.68$ kpc, $Y = 9.57$ kpc and $Z = -0.08$ kpc. The calculated Z value indicates that the cluster King 13 is in the thin Galactic disk. The Galactocentric distance of the cluster is determined as 11.23 kpc.

5. Mass function and dynamical state of King 13

5.1. Luminosity function

The distribution of the stars of an OC based on their brightness is termed as luminosity function. To get the luminosity function, it is very important to know the completeness factor (CF) of CCD data. We implemented the artificial star test for the estimation of CF. To perform this test we have used ADDSTAR routine in DAOPHOT II. We randomly added many stars in different magnitude bins to the original V and I images having the same geometrical positions. We added $\sim 10\%$ of the number of stars actually detected and inserted more stars into fainter magnitude bins. Then we again performed the same procedure of photometry for new images as well. The CF is calculated as the ratio between the number of artificial stars recovered in V and I passbands and the number of added stars per magnitude bin. The values of CF are listed in Table 6 corresponding to each V mag bin. From this table, we can conclude that almost every star has been recovered in the brighter end and as we go towards the fainter end the completeness of the data decreases.

To establish the luminosity function for King 13, we have used V versus $(V-I)$ CMD. Firstly, we converted the apparent V magnitudes of probable member stars into the absolute magnitudes using the value of distance modulus. To remove field star contamination completely from the main sequence of King 13, we used probable cluster members selected by using vector point diagram and parallax. Then we constructed the true histogram of LF as shown in Fig. 11. The histogram shows that the luminosity function for the cluster King 13 rises steadily up to 4.2 mag.

5.2. Mass function

For the main sequence stars, the LF is transformed into the mass function (MF) using the theoretical model given by Bressan et al. (2012). The resulting mass function is plotted in Fig 12.

The mass function slope has been derived by using the relation $\log \frac{dN}{dM} = -(1+x)\log(M) + \text{constant}$, where dN is the number of stars in a mass bin dM with central mass M and x is the slope of MF. The derived MF slope ($x = 1.46 \pm 0.31$) is more precise than Haroon et al. (2014) because the current analysis is based on deep CCD VI data along with GAIA DR2 astrometry. Our derived value of MF slope for this cluster in the mass range $1.1-2.6M_{\odot}$ is in good agreement with the value 1.35 given by Salpeter (1955) for field stars in the Solar neighbourhood.

The Total mass of King 13 was estimated as $\sim 270 M_{\odot}$, considering the derived mass function slope within the mass range $1.1 M_{\odot} - 2.6 M_{\odot}$ and using the following relationship as used by Yadav et al. (2008)

$$M = C \int_{M_L}^{M_U} M^{\Gamma} M dM \quad (5)$$

where C is the constant, M_L and M_U are the upper and lower mass limits of the cluster stars, Γ is the slope of the mass function.

5.3. Dynamical state of the cluster

To characterize the degree of mass-segregation effect in King 13, we plotted the cumulative radial distribution (CRD) of stars for various mass ranges in Fig. 13. The main sequence stars are subdivided into three mass ranges $2.1 \leq \frac{M}{M_{\odot}} < 2.3$, $1.3 \leq \frac{M}{M_{\odot}} < 2.1$ and $0.9 \leq \frac{M}{M_{\odot}} \leq 1.3$. Fig. 13 indicates that more massive stars tend to lie toward the cluster center. The Kolmogorov-Smirnov test ($K - S$) test shows the evidence for statistical significance of this effect with a confidence level of 80 %. CRD of the stars having a mass range $2.1 < \frac{M}{M_{\odot}} \leq 2.3$ can be discriminated from the CRD of fainter stars having mass range $0.9 \leq \frac{M}{M_{\odot}} \leq 1.3$ at a confidence level of 80 %, which clearly shows the evidence of mass-segregation.

Mass segregation effect in clusters may be attributed to dynamical evolution or star formation or both. During the lifetime of a cluster, encounters between its members moderately lead to an increased degree of energy equipartition. At the same time, bright stars gradually sink towards the cluster center and deliver their kinetic energy to the low mass stars, thus leading to this effect. The relaxation time T_E , is the time scale in which the cluster will lose the memory of dynamical initial conditions. Mathematically, T_E is denoted by the following formula (Spitzer and Hart, 1971):

$$T_E = \frac{8.9 \times 10^5 \sqrt{N} \times R_h^{3/2}}{\sqrt{m} \times \log(0.4N)} \quad (6)$$

where N is the number of cluster members, R_h is the half mass radius of the cluster and $\langle m \rangle$ is the mean mass of the cluster stars (Spitzer and Hart, 1971). The value of R_h has been assumed as half of the cluster extent value derived by us. Using the above formula, we have estimated the dynamical relaxation time of King 13 as 7.5 Myr.

The estimated values of relaxation time for this cluster is less than the cluster age. Therefore we conclude that King 13 is a dynamically relaxed cluster.

6. Conclusion

We present a *VI CCD* photometric, 2MASS near-IR and Gaia DR2 astrometric study of the open cluster King 13, which is not well studied in the literature. The estimated fundamental parameters are listed in Table 7. The main results of the present analysis are summarized as follows:

1. To separate cluster members from the field stars, we used Gaia DR2 proper motion and parallax data and obtained a clear main sequence for the cluster. The mean proper motion of the cluster is determined as -2.8 ± 0.2 and -0.9 ± 0.1 mas yr^{-1} in RA and DEC directions respectively.
2. We calculated the structural properties of the cluster. The Center of the cluster is determined as $\alpha = 00^h 10^m 9.6^s$, $\delta_{2000} = 61^\circ 11' 24''$. The Radius and tidal radius of the cluster are determined as 3.2' and 8.5 pc respectively. The value of density contrast parameter δ_c shows that King 13 is a sparse cluster.
3. The values of color-excess ratios $\frac{E(J-K)}{E(V-K)}$ and $\frac{E(J-K)}{E(J-H)}$ are found to be ~ 0.19 and 1.84, which show a normal interstellar extinction in the direction of King 13.
4. From the comparison of the cluster CMDs with theoretical stellar evolutionary isochrones with a metallicity $Z=0.012$ (Bressan et al. (2012)), we determined age, reddening and distance of the cluster as 510 ± 60 Myr, 0.80 ± 0.2 mag and 3.84 ± 0.15 kpc respectively.
5. To study the dynamical properties of cluster, we constructed luminosity and mass function for the cluster. The luminosity function increases towards the fainter end. This indicates that fainter stars are still bound to the cluster. Mass function slope for the cluster is determined as 1.46 ± 0.31 which is in agreement with Salpeter (1955) value. The cumulative radial stellar distribution plot shows presence of mass segregation in the cluster. Dynamical relaxation time of the cluster is found to be 7.5 Myr, which shows that King 13 is a dynamically relaxed cluster.

7. ACKNOWLEDGEMENTS

We thank the staff of ARIES for assistance during observations and data reduction. This work has been partially supported by the Natural Science Foundation of China (NSFC-11590782, NSFC-11421303). This work has made use of data from the European Space Agency (ESA) mission GAIA processed by Gaia Data processing and Analysis Consortium (DPAC, <https://www.cosmos.esa.int/web/gaia/dpac/consortium>).

This publication has made use of data from the 2MASS, which is a joint project of the University of Massachusetts and the Infrared Processing and Analysis Center/California Institute of Technology, funded by the National Science Foundation.

References

- Allen, C., Martos, M.A., 1988. The galactic orbits and tidal radii of selected star clusters. *Rev. Mexicana Astron. Astrofis.* 16, 25–36.
- Bisht, D., Yadav, R.K.S., Durgapal, A.K., 2016. Photometric study of open star clusters in II quadrant: Teutsch 1 and Riddle 4. *New A* 42, 66–77. doi:10.1016/j.newast.2015.06.005.
- Bisht, D., Yadav, R.K.S., Ganesh, S., Durgapal, A.K., Rangwal, G., Fynbo, J.P.U., 2019. Mass function and dynamical study of the open clusters Berkeley 24 and Czernik 27 using ground based imaging and Gaia astrometry. *MNRAS* 482, 1471–1484. doi:10.1093/mnras/sty2781, arXiv:1810.05380.
- Bonatto, C., Bica, E., 2009. The nature of the young and low-mass open clusters Pismis5, vdB80, NGC1931 and BDSB96. *MNRAS* 397, 1915–1925. doi:10.1111/j.1365-2966.2009.14877.x, arXiv:0904.1321.
- Bressan, A., Marigo, P., Girardi, L., Salasnich, B., Dal Cero, C., Rubele, S., Nanni, A., 2012. PARSEC: stellar tracks and isochrones with the PAdova and TRieste Stellar Evolution Code. *MNRAS* 427, 127–145.
- Bukowiecki, Ł., Maciejewski, G., Konorski, P., Strobel, A., 2011. Open Clusters in 2MASS Photometry. I. Structural and Basic Astrophysical Parameters. *Acta Astron.* 61, 231–246. arXiv:1107.5119.
- Cantat-Gaudin, T., Jordi, C., Vallenari, A., Bragaglia, A., Balaguer-Núñez, L., Soubiran, C., Bossini, D., Moitinho, A., Castro-Ginard, A., Krone-Martins, A., Casamiquela, L., Sordo, R., Carrera, R., 2018. A Gaia DR2 view of the open cluster population in the Milky Way. *A&A* 618. doi:10.1051/0004-6361/201833476.
- Cardelli, J.A., Clayton, G.C., Mathis, J.S., 1989. The relationship between infrared, optical, and ultraviolet extinction. *ApJ* 345, 245–256. doi:10.1086/167900.

- Carraro, G., Costa, E., Ahumada, J.A., 2010. Photometric Characterization of the Galactic Star Cluster Trumpler 20. *AJ* 140, 954–961. doi:10.1088/0004-6256/140/4/954, arXiv:1007.4782.
- Durgapal, A.K., Pandey, A.K., 2001. Structure and mass function of five intermediate/old open clusters. *A&A* 375, 840–850. doi:10.1051/0004-6361:20010892.
- Durgapal, A.K., Pandey, A.K., Mohan, V., 1997. CCD photometry of galactic open star clusters - V. King 7. *Bulletin of the Astronomical Society of India* 25, 489.
- Friel, E.D., 1995. The Old Open Clusters Of The Milky Way. *ARA&A* 33, 381–414. doi:10.1146/annurev.aa.33.090195.002121.
- Gaia Collaboration, Prusti, T., de Bruijne, J.H.J., Brown, A.G.A., Valenari, A., Babusiaux, C., Bailer-Jones, C.A.L., Bastian, U., Biermann, M., Evans, D.W., et al., 2016. The Gaia mission. *A&A* 595, A1. doi:10.1051/0004-6361/201629272, arXiv:1609.04153.
- Glushkova, E.V., Zabolotskikh, M.V., Koposov, S.E., Spiridonova, O.I., Vlasyuk, V.V., Rastorguev, A.S., 2010. Photometry of the poorly studied galactic open star clusters King 13, King 18, King 19, King 20, NGC 136, and NGC 7245. *Astronomy Letters* 36, 14–26. doi:10.1134/S1063773710010032.
- Haroon, A.A., Ismail, H.A., Alnagahy, F.Y., 2014. Two MASS photometry of open star clusters: King 13 and Berkeley 53. *Ap&SS* 352, 665–671. doi:10.1007/s10509-014-1990-z.
- Hensy, Y.H.M., 2018. Photometric and astrometric study of open cluster FSR 814 (Koposov 36) using SDSS/2MASS/PPMXL/Gaia DR2. *NRIAG Journal of Astronomy and Geophysics* 7, 180–186. doi:10.1016/j.nrjag.2018.07.006.
- Janes, K.A., Phelps, R.L., 1994. The galactic system of old star clusters: The development of the galactic disk. *AJ* 108, 1773–1785. doi:10.1086/117192.
- Jeffries, R.D., Thurston, M.R., Hambly, N.C., 2001. Photometry and membership for low mass stars in the young open cluster NGC 2516. *A&A* 375, 863–889. doi:10.1051/0004-6361:20010918, arXiv:astro-ph/0107097.

- King, I., 1962. The structure of star clusters. I. an empirical density law. *AJ* 67, 471. doi:10.1086/108756.
- Kumar, B., Sagar, R., Rautela, B.S., Srivastava, J.B., Srivastava, R.K., 2000. Sky transparency over Naini Tal : A retrospective study. *Bulletin of the Astronomical Society of India* 28, 675–686.
- Landolt, A.U., 1992. UBVRI photometric standard stars in the magnitude range 11.5 \leq V \leq 16.0 around the celestial equator. *AJ* 104, 340.
- Lynge, G., 1982. Open clusters in our Galaxy. *A&A* 109, 213–222.
- Marx, S., Lehmann, H., 1979. Three color photometry of the open cluster AN King 13. *Astronomische Nachrichten* 300, 295–300. doi:10.1002/asna.19793000607.
- Mathis, J.S., 1990. Interstellar dust and extinction. *ARA&A* 28, 37–70. doi:10.1146/annurev.aa.28.090190.000345.
- Pandey, A.K., Durgapal, A.K., Bhatt, B.C., Mohan, V., Mahra, H.S., 1997. Stellar contents of the open clusters Be 64 and Be 69. *A&AS* 122, 111–121. doi:10.1051/aas:1997296.
- Persson, S.E., Murphy, D.C., Krzeminski, W., Roth, M., Rieke, M.J., 1998. A New System of Faint Near-Infrared Standard Stars. *AJ* 116, 2475–2488. doi:10.1086/300607.
- Piskunov, A.E., Kharchenko, N.V., Röser, S., Schilbach, E., Scholz, R.D., 2006. Revisiting the population of Galactic open clusters. *A&A* 445, 545–565. doi:10.1051/0004-6361:20053764, arXiv:astro-ph/0508575.
- Rangwal, G., Yadav, R.K.S., Durgapal, A., Bisht, D., Nardiello, D., 2019. Astrometric and photometric study of NGC 6067, NGC 2506, and IC 4651 open clusters based on wide-field ground and Gaia DR2 data. *MNRAS* 490, 1383–1396. doi:10.1093/mnras/stz2642, arXiv:1909.08810.
- Riess, A.G., Casertano, S., Yuan, W., Macri, L., Bucciarelli, B., Lattanzi, M.G., MacKenty, J.W., Bowers, J.B., Zheng, W., Filippenko, A.V., Huang, C., Anderson, R.I., 2018. Milky Way Cepheid Standards for Measuring Cosmic Distances and Application to Gaia DR2: Implications for the Hubble Constant. *ApJ* 861, 126. doi:10.3847/1538-4357/aac82e, arXiv:1804.10655.

- Salpeter, E.E., 1955. The Luminosity Function and Stellar Evolution. *ApJ* 121, 161. doi:10.1086/145971.
- Spitzer, Jr., L., Hart, M.H., 1971. Random Gravitational Encounters and the Evolution of Spherical Systems. I. Method. *ApJ* 164, 399. doi:10.1086/150855.
- Stetson, P.B., 1987. DAOPHOT - A computer program for crowded-field stellar photometry. *PASP* 99, 191–222. doi:10.1086/131977.
- Subramaniam, A., Bhatt, B.C., 2007. Photometric study of distant open clusters in the second quadrant: NGC 7245, King 9, King 13 and IC 166. *MNRAS* 377, 829–834. doi:10.1111/j.1365-2966.2007.11648.x, arXiv:astro-ph/0703075.
- Yadav, R.K.S., Kumar, B., Subramaniam, A., Sagar, R., Mathew, B., 2008. Optical and near-infrared photometric study of the open cluster NGC 637 and 957. *MNRAS* 390, 985–996. doi:10.1111/j.1365-2966.2008.13740.x, arXiv:0810.1409.

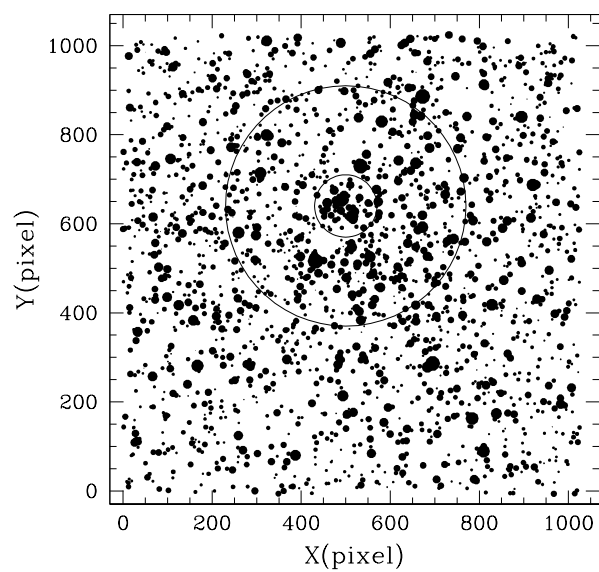


Figure 1: Identification chart of the stars in the cluster and field regions of King 13. North is up and East in the right direction. The outer circle represents the extent of the cluster while the inner circle shows the extent of core of the cluster. The smallest size denotes star of $V \sim 20$ mag.

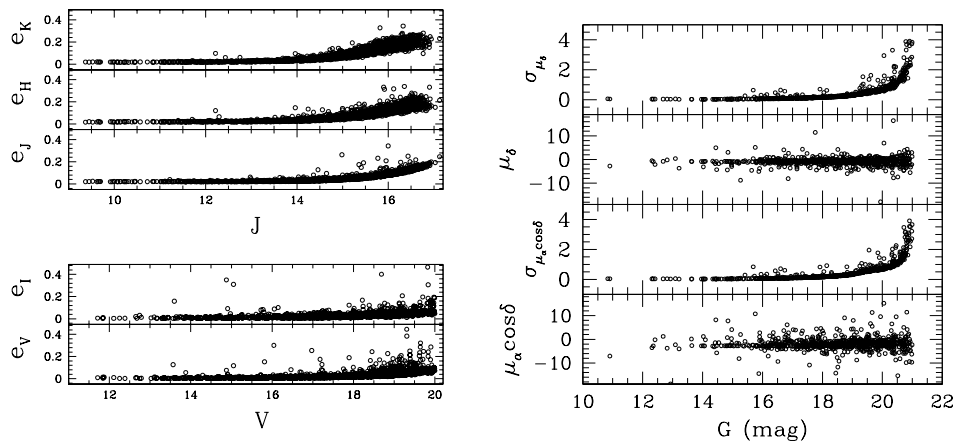


Figure 2: Left panel shows photometric errors in V and I magnitudes against V magnitude and errors in J , H and K magnitudes against J magnitudes. Right **panel** shows the plot of proper motions in both RA and DEC directions and their errors versus G magnitude.

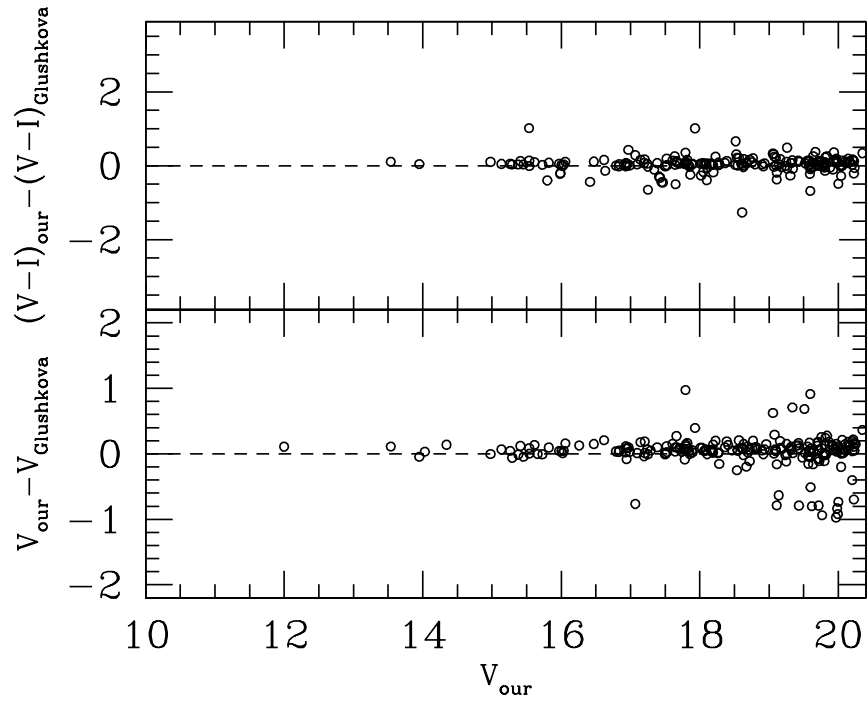


Figure 3: A comparison of the present photometry with photometric data of Glushkova et al. (2010) for King 13. The open circles represent difference of both the photometries as a function of present photometry.

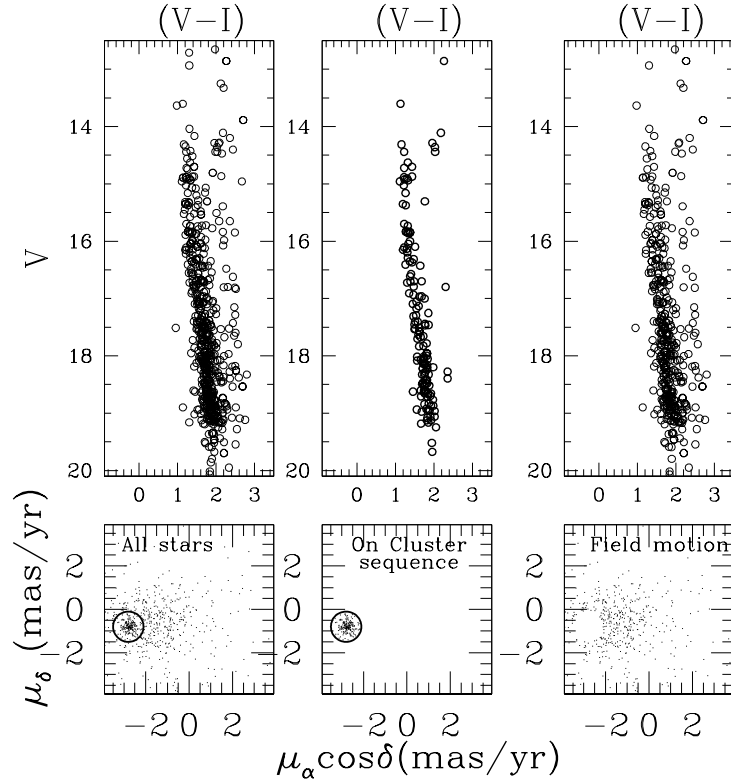


Figure 4: Colour magnitude diagrams (CMDs) based on our VI photometry (top panels) and proper motion vector point diagrams (VPDs) based on *Gaia* DR2 data (bottom panels). Left panels display the entire sample. Central panels display the candidate members (enclosed in a circle of radius 0.7 mas yr^{-1} around the cluster center in VPD). Probable background/foreground field stars in the direction of the cluster are displayed in the right panels.

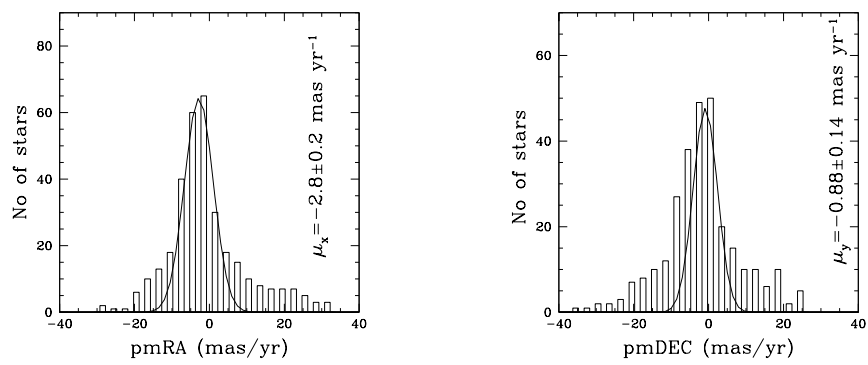


Figure 5: The histograms for proper motion in right ascension (left) and declination (right). The Gaussian function fit to the central bins provides the mean values in RA and DEC. panels.

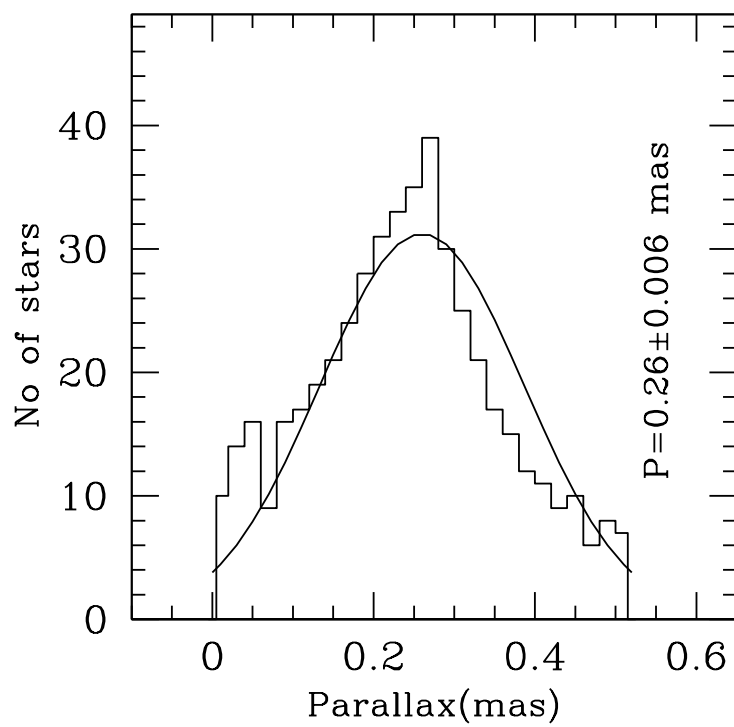


Figure 6: The histograms for the estimation of mean parallax. The Gaussian function fit to the central bins.

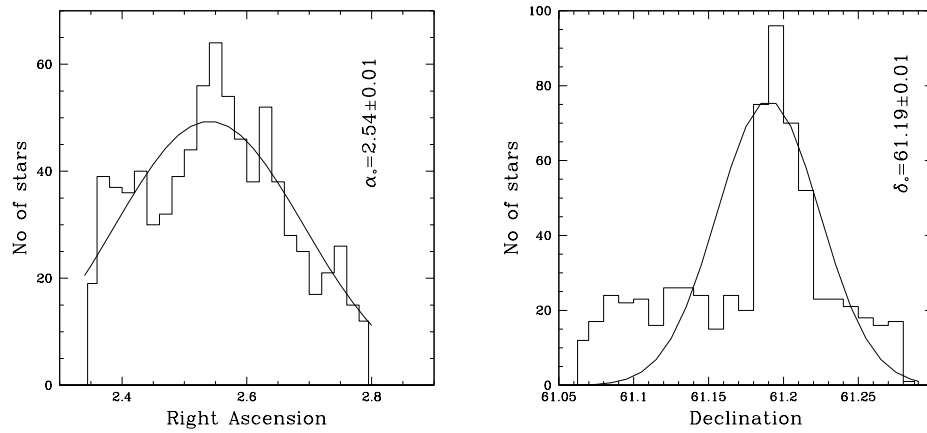


Figure 7: The histograms for the estimation of center coordinates. The Gaussian function fit to the central bins provides cluster center.

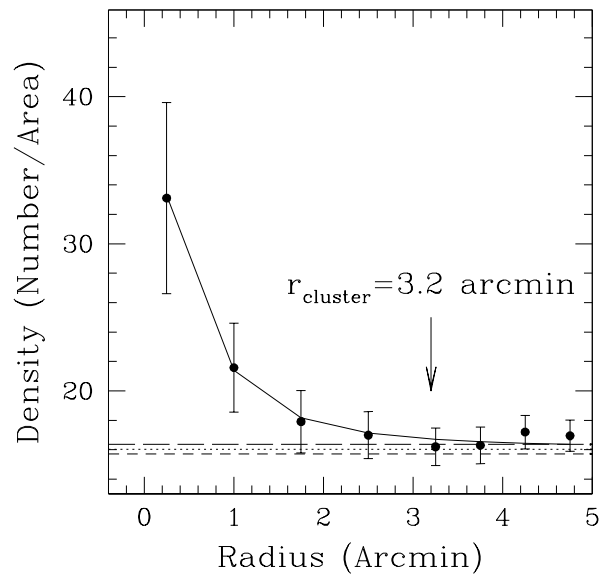


Figure 8: Surface density distribution of stars in the field of the cluster King 13. Errors are determined from sampling statistics ($=\frac{1}{\sqrt{N}}$ where N is the number of stars used in the density estimation at that point). The smooth line represent the fitted profile whereas dotted line shows the background density level. Long and short dash lines represent the errors in background density.

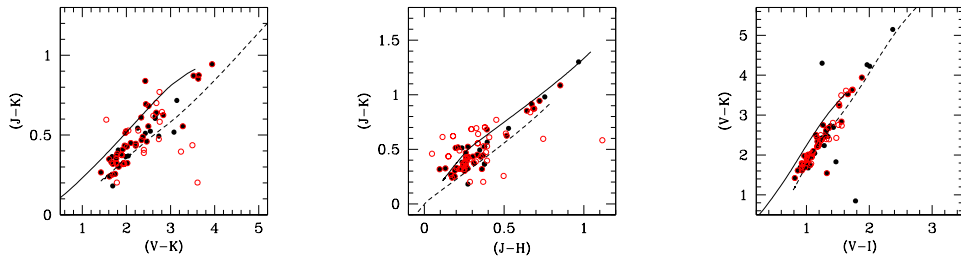


Figure 9: The $(J - K)$, $(V - K)$, $(J - K)$, $(J - H)$ and $(V - I)$, $(V - K)$ colour-colour diagrams for the cluster King 13. The solid line is the ZAMS taken from Bressan et al. (2012). The dotted line is the ZAMS shifted by the values given in the text. Red open circles are matched stars with Cantat-Gaudin et al. (2018) having membership probability higher than 0.5.

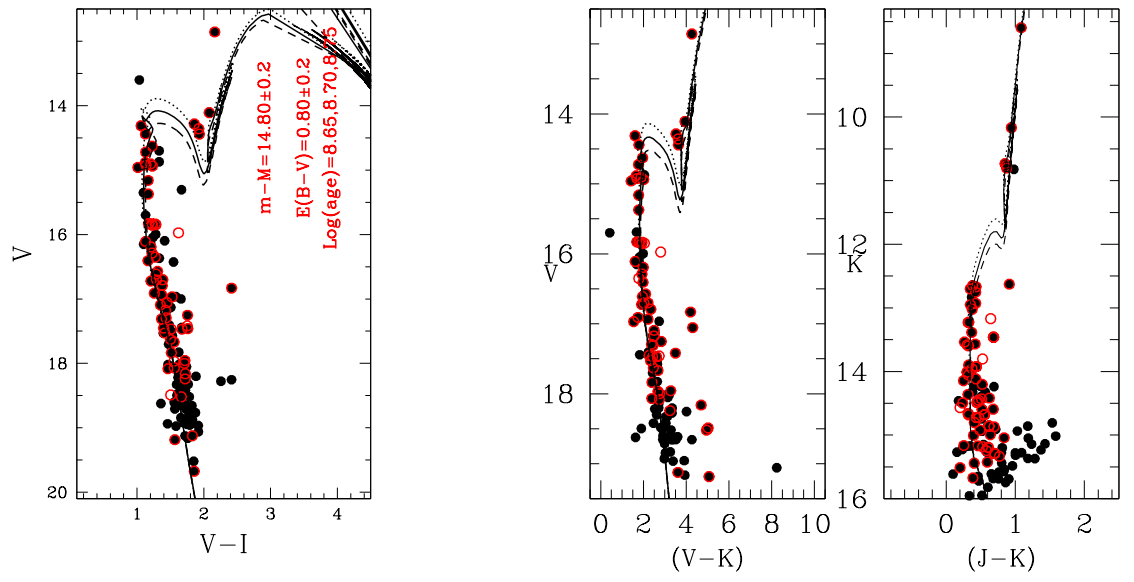


Figure 10: The V , $(B - V)$, V , $(V - K)$ and K , $(J - K)$ colour-magnitude diagram of the cluster King 13. The curves are the isochrones of $(\log(\text{age}) = 8.65, 8.70 \text{ and } 8.75)$. These isochrones are taken from Bressan et al. (2012). Red open circles are matched stars with Cantat-Gaudin et al. (2018) having membership probability higher than 0.5.

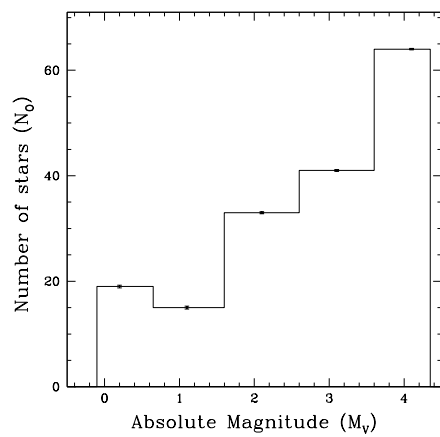


Figure 11: The luminosity functions of the cluster under consideration.

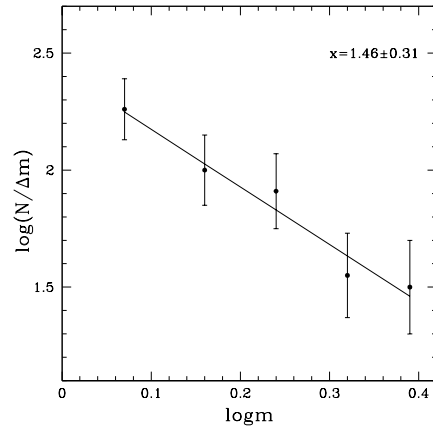


Figure 12: Mass function for King 13 derived using Bressan et al. (2012) isochrones. Standard deviations from the central values are represented by the error bars.

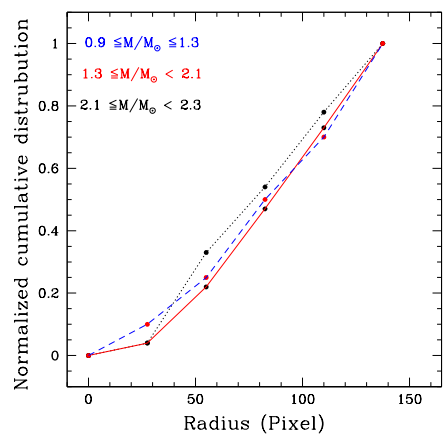


Figure 13: The cumulative radial distribution of stars in various mass range.

Table 1: Log of observations for the cluster under study. King 13 was observed on 2nd December 2014.

Pass band	Exposure Time (in seconds)
<i>V</i>	240×2, 120×2
<i>I</i>	120×2, 60×2

Table 2: Derived Standardization coefficients and its errors. C and Z are color coefficients and zeropoints respectively.

Filter	C	Z
V	-0.09 ± 0.004	4.84 ± 0.008
I	-0.11 ± 0.008	5.35 ± 0.009

Table 3: The rms global photometric errors as a function of V magnitude.

V	σ_V	σ_I
14 – 15	0.04	0.05
15 – 16	0.04	0.06
16 – 17	0.05	0.08
17 – 18	0.06	0.09
18 – 19	0.06	0.10
19 – 20	0.07	0.12

Table 4: Differences in V and $(V - I)$ between Glushkova et al. (2010) and our study. The standard deviation for the difference in each magnitude bin is also given in the parentheses.

V	ΔV	$\Delta(V - I)$
13 – 14	-0.01 (0.01)	0.02 (0.02)
14 – 15	-0.02 (0.02)	-0.02 (0.04)
15 – 16	-0.04 (0.04)	-0.03 (0.05)
16 – 17	-0.05 (0.05)	-0.05 (0.07)
17 – 18	-0.07 (0.07)	0.06 (0.10)
18 – 19	-0.08 (0.08)	0.07 (0.12)
19 – 20	-0.10 (0.10)	0.09 (0.13)

Table 5: Structural parameters of the cluster King 13. Background and central density are in the unit of stars per arcmin². r_c is in arcmin while R_t is in pc.

Name	f_0	f_b	r_c	R_t	δ_c
King 13	36.3	16.04	0.6	8.5	2.8

Table 6: The photometric completeness of the data in each magnitude bin for the cluster King 13.

V (mag)	Completeness
14 - 15	0.99
15 - 16	0.97
16 - 17	0.95
17 - 18	0.91
18 - 19	0.75

Table 7: Various fundamental parameters of the cluster King 13.

Parameter	King 13
Radius	3.2 arcmin
Right Ascension	2.54 ± 0.01 deg
Declination	61.19 ± 0.01 deg
$\mu_{\alpha\cos\delta}$	-2.8 ± 0.2 mas yr ⁻¹
μ_{δ}	-0.9 ± 0.1 mas yr ⁻¹
Age	510 ± 60 Myr
[Fe/H]	-0.03 ± 0.01 dex
Metal abundance	0.012
$E(G_{BP} - G_{RP})$	0.71 ± 0.26
E(B-V)	0.80 ± 0.2 mag
A_V	2.43
R_V	3.04
Distance modulus	14.80 ± 0.20 mag
Distance (From Isochrone fitting)	3.75 ± 0.40 Kpc
Distance (From mean Parallax)	3.84 ± 0.15 Kpc
X_{\odot}	3.68 kpc
Y_{\odot}	9.57 kpc
Z_{\odot}	-0.08 kpc
R_{GC}	11.23 kpc
Total Luminosity	~ 4.2 mag
Cluster members	172
IMF slope	1.46 ± 0.31
Total mass	$\sim 270M_{\odot}$
Average mass	$1.56M_{\odot}$
Relaxation time	7.5 Myr